Control of contextual memory through interneuronal α5-$GABA_A$ receptors

Mengwen Zhu[1], Alifayez Abdulzahir[1], Mark G. Perkins[1], Bryan M. Krause[1], Richard Lennertz[1], David Ruhl[2†], Harald Hentschke[3], Rajasekar Nagarajan[4], Edwin R Chapman[2], Uwe Rudolph[4,5], Michael S Fanselow[6], Robert A Pearce[1]*

[1]Department of Anesthesiology, University of Wisconsin-Madison; Madison, WI, USA

[2]Department of Neuroscience, University of Wisconsin-Madison; Madison, WI, USA

[3]Freelance Data Scientist, Berlin, Germany

[4]Department of Comparative Biosciences, University of Illinois at Urbana-Champaign; Urbana, IL, USA

[5]Carl R. Woese Institute for Genomic Biology, University of Illinois at Urbana-Champaign, Urbana, IL, USA

[6]Departments of Psychology and Psychiatry, University of California, Los Angeles; Los Angeles, CA, USA

†Present address: Neurocrine Biosciences, San Diego, CA, USA

*Corresponding author: rapearce@wisc.edu

Abstract: γ-aminobutyric acid type A receptors that incorporate α5 subunits (α5-$GABA_A$Rs) are highly enriched in the hippocampus and they are strongly implicated in the control of learning and memory. Receptors located on pyramidal neuron dendrites have long been considered responsible, but here we report that selective elimination of α5-$GABA_A$Rs from either interneurons or pyramidal cells prevented the general anesthetic etomidate from suppressing contextual learning. Using Ca^{2+} imaging of hippocampal neuronal activity in freely exploring mice, we also found that etomidate interfered with the development of place cells and spatial engrams in wild type mice but not in interneuron-specific α5-$GABA_A$R knockout mice. These findings show that α5-$GABA_A$Rs on interneurons as well as pyramidal neurons mediate etomidate-induced amnesia.

Word count: 4097 (main text, excluding abstract, methods, references, and figure legends)

Introduction

Inhibitory synaptic transmission in the brain is mediated primarily by γ-aminobutyric acid type A receptors ($GABA_A$Rs). This family of chloride-permeable ionotropic receptors is the target of a wide variety of clinically important agents, including sedative-hypnotics, anxiolytics, anticonvulsants, and general anesthetics [1,2]. Many of these agents also impair memory. Usually this is an undesired side-effect, but for general anesthetics it is a primary goal. Indeed, awareness with recall during anesthesia is recognized as a persistent problem [3-5], and it has been associated with dysphoria and post-traumatic stress disorder [4,6]. In studies of the mechanism of anesthetic-induced amnesia, etomidate has proved exceptionally useful, in part because it is highly selective for $GABA_A$ receptors, but also because its physicochemical properties make it amenable to use both *in vivo* and *in vitro* [7,8].

Etomidate potently blocks memory formation even at subanesthetic doses by targeting $GABA_A$Rs that incorporate α5 subunits (α5-$GABA_A$Rs) [9,10]. These receptors are highly concentrated in the hippocampus [11,12], a brain structure that is essential for the formation of episodic memories [13]. The well-established role of α5-$GABA_A$Rs in learning and memory has prompted the development of agents that target α5-$GABA_A$Rs to enhance cognition [14-18], with application to diverse disease states including Alzheimer's disease, Down syndrome, autism, depression, and schizophrenia [16,19-26].

The generally accepted mechanism by which α5-$GABA_A$Rs modulate memory involves receptors at extrasynaptic sites on pyramidal neuron dendrites, their predominant site of expression [27]. Indeed, acting through slow phasic inhibition, dendritic receptors are well suited to prevent the depolarization and NMDAR-mediated calcium entry that initiates synaptic plasticity [28]. Accordingly, GABAergic drugs such as etomidate that are normally able to suppress long-term potentiation (LTP) and learning are ineffective in mice with a global knockout of α5 subunits (α5-KO), or in mice administered α5-selective negative modulators [9,10]. However, recent studies indicate that α5-$GABA_A$Rs are not restricted to pyramidal neurons [29,30], and we found that selective knockout of α5 subunits from pyramidal neurons did not recapitulate the global α5-KO phenotype [31]. Moreover, suppression of LTP and contextual fear conditioning were independent of $GABA_A$Rs that incorporate β3 subunits, which underlie tonic and long-lasting phasic inhibition in pyramidal neurons [32,33]. These findings raised the possibility that α5-$GABA_A$Rs on pyramidal neurons might not be the only targets that underlie etomidate-induced amnesia, or that mediate the enhancement of spatial memory by agents that selectively inhibit α5-$GABA_A$Rs [24,34]. In the present study we tested whether α5-$GABA_A$Rs on interneurons might also be responsible, by creating and testing novel interneuron-selective α5-$GABA_A$R knockout (α5-i-KO) mice.

Results

α5-$GABA_A$R loss is specific to interneurons

To generate mice lacking α5-$GABA_A$Rs specifically in interneurons, we crossed mice carrying a floxed α5 allele (Gabra5$^{tm2.1Uru}$) with mice that express Cre recombinase under the control of the Gad2 promoter (Gad2$^{tm2(cre)Zjh}$) (Fig. 1A). Western blot analysis showed that both male and female Cre- (pseudo-wild type: p-WT) and Cre+ (α5-i-KO) mice expressed α5 subunits at levels indistinguishable from C57BL/6J WT mice, consistent with the predominant expression of α5-$GABA_A$Rs in pyramidal neurons and their selective knockout from interneurons (Fig. 1, B and C). To exclude the possible involvement of astrocytes, which also express $GABA_A$Rs and synthesize and release GABA [35], we also tested for co-expression of cre-

driven tdTomato reporter and GFAP-driven GFP (Fig. 1D). We found complete segregation of the markers (Fig. 1E), further supporting the restriction of α5 subunit knockout to interneurons.

Hippocampus-dependent contextual memory is not blocked by etomidate in α5-i-KO mice

To test whether interneuronal α5-$GABA_A$Rs are essential to etomidate's suppression of hippocampus-dependent memory, we employed the Context Preexposure Facilitation Effect (CPFE) learning paradigm (Fig. 1E) – a variant of contextual fear conditioning that separates the contextual learning and aversive phases of conditioning [36-39]. This paradigm takes advantage of the "immediate shock deficit" [40], wherein mice that are shocked immediately after they are placed in a novel context fail to associate the context and shock, whereas mice that were pre-exposed to the context on the preceding day recall the context rapidly and successfully associate it with the shock [41,42]. Because the drug is present only during contextual learning (day 1) and not when the shock is administered (day 2), any observed change in freezing behavior (day 3) can be attributed to a failure to learn the context rather than an attenuation of the shock's effectiveness. There were no baseline differences between p-WT and α5-i-KO mice in anxiety, as indicated by open arm entries or open arm time in the elevated plus maze test, or in pain sensitivity, as indicated by time to withdrawal in the hot plate test (Fig. S1). Etomidate produced equal levels of sedation in the two genotypes, as indicated by immobility during context pre-exposure (Fig. 1F, *left*; 2-way ANOVA, genotype x drug interaction factor, $F(1,44) = 0.126$, $p = 0.72$). Mice that had been pre-exposed to context displayed greater freezing than mice that had not been pre-exposed, demonstrating effective contextual learning (data not shown). However, etomidate differentially suppressed freezing between the two genotypes (Fig. 1F, *right*; 2-way ANOVA, genotype x drug interaction factor $F(1,44) = 11.08$, $p=0.0018$): freezing was strongly suppressed in p-WT mice ($t(44)=5.46$, $p<0.001$, Sidak's multiple comparison test) but not in α5-i-KO mice ($t(44)=0.75$, $p=0.70$). These results demonstrate that α5-$GABA_A$Rs on interneurons are essential for suppression of contextual conditioning by a sedative dose of etomidate.

To determine the contribution of α5-$GABA_A$Rs on pyramidal neurons to etomidate's suppression of hippocampus-dependent memory, we also performed CPFE experiments in mice lacking α5-$GABA_A$Rs specifically in pyramidal neurons (α5-pyr-KO). To generate these mice, we crossed mice carrying a floxed α5 allele ($Gabra5^{tm2.1Uru}$) with mice that express Cre recombinase under the control of the CamK2a promoter [43]. Etomidate produced similar levels of sedation in p-WT and α5-pyr-KO mice (Fig. 1G, *left*; 2-way ANOVA, genotype x drug interaction factor, $F(1,61) = 0.194$, $p = 0.66$). Interestingly, etomidate again suppressed freezing differently between the two genotypes (Fig. 1G, *right*; 2-way ANOVA, genotype x drug interaction factor $F(1,61) = 14.2$, $p=0.0004$). Freezing was strongly suppressed in p-WT mice ($t(61) = 5.06$, $p < 0.0001$, Sidak's multiple comparison test) but not in α5-pyr-KO mice ($t(61)=0.233$, $p = 0.97$), similar to our results with the α5-i-KO mice. This finding indicates that etomidate also engages pyramidal neuron α5-$GABA_A$Rs to block memory, consistent with previous experiments linking these receptors on CA1 pyramidal neurons specifically to control of spatial memory [44].

Etomidate suppresses place cell formation via interneuronal α5-$GABA_A$Rs

The hippocampus supports contextual memory by forming a cognitive map of the environment [45,46]. Spatially modulated firing of individual cells, referred to as 'place cells', contribute to that map [47,48]. Their spatial specificity can be stable for periods of days or even weeks in a given environment [49,50], but they undergo 'remapping' when the animal is placed in a

new environment [51,52]. Although not every place cell is seen again upon re-exposure to the same environment, when it is reactivated, its place field is retained [53]. Therefore, as an ensemble, the formation and re-activation of place cells can serve as a 'readout' of the encoded contextual memory, stable over a period of weeks [54].

To test the influence of etomidate on this process, and whether it depends on α5-$GABA_A$Rs on interneurons, we measured the spatially modulated firing characteristics of CA1 pyramidal neurons in p-WT and α5-i-KO mice (Figs. 2,3). We tracked the activity of individual neurons for up to twelve weeks as mice were exposed to novel contexts two to three times per week [55]. To assess place cell activity, we injected virus carrying the genetically encoded calcium indicator GCaMP6f driven by the CaMKIIa promoter (AAV1-CaMKIIa-GCaMP6f) into the dorsal hippocampus of 8 mice (4 WT, 4 α5-i-KO). Two to three weeks later, a gradient refractive index (GRIN) lens and baseplate were attached to the skull, to which was affixed a miniature endoscope (nVoke2, Inscopix, Palo Alto, CA). Beginning ~4-6 weeks after virus injection, abundant transient fluorescent signals were observed in up to 850 individual CA1 pyramidal neurons in a freely exploring mouse (Fig. 2A; Fig. S2). The Ca^{2+} event rates over the course of a 10-minute period of exploration averaged ~0.1 min^{-1} (Fig. 2B), similar to previous reports [53,56]. Event rates were slightly lower overall in α5-i-KO mice (2-way ANOVA, genotype effect $F(1,12)=8.86$, $p=0.012$) but they were not altered by etomidate (drug effect $F(1,12)=0.11$, $p=0.74$) and genotype did not influence the (lack of) effect of etomidate (genotype x drug $F(1,12)=0.17$, $p=0.68$).

To quantify place-specific firing of individual neurons, we simultaneously monitored the position of the mouse using video tracking software (Noldus EthoVision XT15) together with endoscopic fluorescent report of cellular activity (Inscopix Data Acquisition Software 2019). Fig. 2C shows an example of one such experiment. The track of the mouse over the 10-min exploration is shown by the purple line, with dots superimposed over the rising phase of detected calcium spikes (Fig. 2C, left panel). This information was used to create a map of firing rate as a function of position (Fig 2C, middle panel). To quantify the place-specificity of cellular activity, we calculated the mutual information (MI) between firing rate and arena location and compared it to a null distribution produced by 1000 time-shuffled rate maps (Fig. 2C, right panel; Fig. S3(A)). Using the criterion that the probability of the observed MI value must fall within the top 5% of the null distribution (i.e. $p(MI) < 0.05$) for a cell to be considered a "place cell", we found that 16% of all cells in p-WT mice were place cells, consistent with previous reports [53].

To determine whether an amnestic dose of etomidate altered place cell formation during a 10-minute exploratory session in a novel environment – matching the pre-exposure phase of CPFE (Fig. 1F) – we administered saline (control) or etomidate (7 mg/kg IP) 30 minutes prior to placing the mouse in the experimental arena and recording Ca^{2+} transients and mouse position. Examples of activity tracks and Ca^{2+} event rate maps are shown in Fig. 2D, for p-WT (left) and α5-i-KO mice (right). For each session we measured the fraction of cells with $p(MI)<0.05$. We repeated this experiment 3-6 times for each mouse, presenting different sets of contextual cues each day. Histograms of p(MI) values combined across all experiments are presented in Fig. 2E, and the fraction of place cells (PC_{prob}) seen in each mouse after saline or etomidate in Fig. 2F. The population of cells with low p(MI) was essentially eliminated by etomidate in p-WT mice (Fig. 2E, top; Fig. 2F, left), but reduced to a smaller extent in α5-i-KO mice ($\chi2(1) =3.92$, $p=0.048$; PC_{prob} ~ genotype x drug + (1|mouseID)). This finding – that place cell suppression depends on α5-$GABA_A$Rs on interneurons – thus mirrors our CPFE results (Fig. 1), supporting a causal link between etomidate interference with place cell formation and contextual learning.

Etomidate suppresses spatial engrams via interneuronal α5-GABA$_A$Rs

Once formed, place cells can remain stable for days to weeks, displaying the same position-specific activity upon repeated exposure to the same environment [54], thereby forming a memory trace, or 'spatial engram', of the environment. Cells that do not meet the relatively strict criterion of p(MI)<0.05 also carry some spatial information and contribute to the spatial engram [54,57,58]. Therefore, to test the influence of etomidate on spatial engram formation and stability, we compared the similarity between firing patterns during an initial exposure to a novel environment in an 'AM session' versus re-exposure to that same environment during a 'PM session' 4 hours later (Fig. 3A), using Ca^{2+} event rate maps from all cells that were active during both sessions. We quantified the similarity in spatially modulated activity in two ways: first, on a cell-by-cell basis, by computing the Pearson's correlation coefficient (PCC) between rate maps (RMs) for AM and PM sessions; and secondly, on an ensemble basis, by computing the PCC between population vectors (PVs) of firing rates of all cells at each position in the arena. The probabilities that all active cells and place cells that were seen in the AM session would also be seen in the PM session are presented in Fig. S4, and examples of rate maps and their associated RM correlation values (RM_{corr}) from paired AM/PM sessions are shown in Fig. 3B. These cells exemplified the activity patterns that we observed: under control conditions (saline), when p-WT mice were returned to the arena with the same contextual cues in the afternoon, cells tended to fire in the same spatial locations. However, if mice had received etomidate prior to the AM session, cells 'remapped' to new locations. By contrast, α5-i-KO mice maintained consistent spatial activity patterns regardless of drug condition. Fig. 3C shows the distribution of RM_{corr} values for all cells in paired AM/PM sessions, after injection of saline or etomidate (7 mg/kg). RM_{corr} values fell largely outside the location-shuffled null distribution (dashed lines) after saline; etomidate caused the distribution to be shifted to the left in p-WT mice but not in α5-i-KO mice. The same pattern of responses was also seen for PV_{corr} values (Fig. 3D). Combined results from all mice administered saline or etomidate (7 mg/kg) are presented in Fig. 3E (RM_{corr} left, PV_{corr} right). Each point represents the average of 3-6 paired AM/PM sessions for each mouse under each condition. Etomidate significantly reduced RM_{corr} and PV_{corr} (RM_{corr}, $t(56) = -4.57$, $p<0.001$; PV_{corr}, $t(47.6)=-3.64$, $p<0.001$; RM_{corr} ~ fixed effects genotype x drug, random effects mouse identity + recording session + cell identity; PV_{corr} ~ fixed effects genotype x drug, random effects mouse identity + recording session), and though there was no significant difference between genotypes with saline (RM_{corr}, $t(8.9) = -0.31$, $p=0.76$; PV_{corr} $t(9.0) = -2.58$, $p=0.80$) the effect was reversed in α5-i-KO mice (significant genotype x drug interactions: RM_{corr}, $\chi^2(1) =5.08$, $p=0.024$; PV_{corr}, $\chi^2(1) =4.58$, $p=0.032$). Similar experiments using etomidate doses of 2, 4, 6, and 8 mg/kg IP, but with a single pair of AM&PM sessions for each mouse at each dose, showed that etomidate caused dose-dependent reductions in RM_{corr} and PV_{corr} that were attenuated in α5-i-KO mice (Fig. S5). Fig. 3F presents the linear mixed effects model (LMEM) estimates and 95% confidence intervals (CIs) for etomidate modulation of RM_{corr} at all doses, showing significant effects of etomidate and interactions between drug and genotype at doses above 4 mg/kg. These results show that in addition to interfering with place cell formation, etomidate suppresses spatial engram formation and/or stability through α5-GABA$_A$Rs on interneurons.

To confirm that the RM and PV correlations reflect the formation of spatial engrams specific to the set of contextual cues presented during the AM session, we conducted an additional series of studies using alternate contexts between AM and PM sessions following

saline administration (Fig. 4A,B). RM and PV values were indeed significantly lower in p-WT mice when the contextual cues had been changed (RM_{corr}, $\chi^2(1) = 10.4$, $p=0.0013$; PV_{corr}, $\chi^2(1) = 4.3$, $p=0.038$; RM_{corr} ~ fixed effects genotype x context, random effects mouse identity + recording session + cell identity; PV_{corr} ~ fixed effects genotype x context, random effects mouse identity + recording session), and there was a trend toward reduction in α5-i-KO mice (RM_{corr}, $\chi^2(1) = 3.6$, $p=0.057$; PV_{corr}, $\chi^2(1) = 3.0$, $p=0.083$). These findings support the use of PV and RM correlations as cellular correlates of spatial memory.

Although the distributions of both RM and PV correlations were reduced in altered-context compared to same-context AM&PM experiments, they still were significantly higher than their location-shuffled null distributions (Fig. 4B, null). These 'residual correlations' suggest that some component of the hippocampal activity pattern reflects a more general aspect of the environment, such as the room in which experiments were conducted or the plexiglass arena surrounded by a blackout curtain into which they were placed, as opposed to the unique sensory cues within the arena that constituted the 'context' [59]. Because we presented a new set of cues every experimental day, we were able to conduct analyses analogous to the altered-context experiments by treating each pair of PM sessions on different days as different experiments (Fig. 4C). We found that the mean correlation values were higher for pairs of days that were closer in time (shown by brighter colors closer to the diagonal of identity in Fig. 4C), in both genotypes. Plots of the mean PV correlations as a function of time between sessions showed that the mean residual correlations between days close in time matched the residual correlations from altered-context experiments (PM_{mean} and RM_{mean} ~0.2), but that it fell to '0' (~ the mean of the null distribution) for sessions separated by approximately two months (Fig 4D). Based on these findings, we speculate that engrams are formed by a combination of experimentally altered 'unique contextual' cues and unaltered 'general environmental' cues (i.e. different levels in a hierarchical memory system [60]), and that the representation of the environment drifts over a time frame corresponding to slow components of system consolidation [61].

We conducted a final set of experiments similar to the AM/PM experiments but using WT mice and pairs of sessions separated by 24 hours rather than 4 hours, to test whether correlations seen at 4 hours remain stable over 24 hours. RM and PV correlations were essentially identical (Fig. S6), indicating that the spatial engrams measured at 4 hours provide a good measure of their strength at 24 hours – a more typical measure of long-term memory in behavioral studies, including those that we used for CPFE tests of memory (Fig. 1).

Discussion

Results from both behavioral and functional imaging experiments demonstrated that α5-$GABA_A$Rs on interneurons are essential targets for learning suppression by the archetypal GABAergic general anesthetic etomidate. The calcium imaging results provided additional mechanistic insight, showing that etomidate suppresses the initial development of place cells and interferes with the formation and/or stability of a spatial engram encoded by a combination of place cells and non-place cells. This conclusion challenges the longstanding and widely accepted model of memory modulation through α5-$GABA_A$R-mediated tonic and slow phasic inhibition on pyramidal neurons [28,62-64]. The finding that etomidate must act simultaneously on both interneurons *and* pyramidal neurons to suppress contextual learning suggests that the memory-forming circuitry of the hippocampus is relatively robust: memories can be formed even in the face of enhanced inhibition of pyramidal neuron dendrites, or when plasticity-promoting disinhibition is disrupted. That is, the two plasticity-promoting mechanisms may provide a

measure of redundancy. However, when etomidate simultaneously modulates α5-$GABA_A$Rs at both locations, it is able to suppress memory formation.

The methods we used – repeatedly exposing mice to novel sets of contextual cues several times per week for up to twelve weeks – provided robust cellular correlates of spatial memory, and they allowed us to develop full dose-response relationships from groups of only four mice of each genotype. Not only should this approach be applicable to a wide range of questions, but it also has the added benefits of efficient resource utilization and minimization of animal welfare concerns by reducing the total number of animals used.

Here we have used the term "spatial engram" to refer to the correspondence between the recurrence of spatially modulated neuronal activity patterns (Fig. 3) and the formation or suppression of hippocampus-dependent contextual memories (Fig. 1). In this regard, spatial engrams incorporate characteristics of both place fields as cognitive maps [45,65] and engrams as revealed and captured by the activation of learning-related immediate early genes (IEGs, including c-Fos, ARC, and NPAS4), and replayed through optogenetic activators [66]. However, spatial engrams differ from place cell maps and IEG-defined engrams in several important ways: i) they include both place cells and non-place cells; ii) they presumably include both engram cells and non-engram cells [67]; and iii) they represent ensemble activity of a large proportion of the population – perhaps up to one-half, as indicated by the bimodal distributions of cells that fall within or outside the null distributions (Fig. S5) – rather than a restricted subset (~3%) of highly active cells. These spatially modulated firing patterns, which other investigators who have used the same recording methods have also observed [53,54,59], embody many of the characteristics expected of neuronal correlates of memory. These include the ability to retain stable representations of an environment over extended periods of time [53,59], the ability to discriminate between arenas with different cues but at the same time to generalize between arenas in the same general environment [59] (and Fig. 4A), and fluctuating activity patterns that create unique episodic time stamps [68]. Here we add to this collection of attributes the finding that a drug that prevents learning also directly interferes with the development of stable neuronal ensembles – thus extending it from a set of correlations to include an interventional test. Admittedly, these findings do not yet match the extensive evidence developed over the past decade indicating that IEG-captured engram cells represent the physical substrate of memories themselves [66]. To develop a comparable level of evidence would require reinstating the activity of the entire ensemble in a manner that drives memory-guided behavior, but such a method has not yet been developed. Nevertheless, it is likely that spatial engrams do include IEG-captured engram cells, so ecphory might well be seen, but this point is speculative. Furthermore, just as a set of bona-fide engram cells observed in the hippocampus or elsewhere in the brain does not constitute an entire memory trace but is just one portion of an engram complex [69], the spatial engrams that we describe here are likely one component of a memory trace that extends across multiple structures [70], to capture the memory of the arena, the general environment, and the context within which the experiments take place.

Which types of interneurons might be responsible for the present findings? It is counterintuitive that suppressing interneuron activity through positive modulation of their α5-$GABA_A$Rs would impair memory – at least if one considers inhibitory interneurons only in terms of controlling the depolarization of pyramidal neurons. Reducing this constraining influence would instead lead to net disinhibition, enhancing the ability of pyramidal neurons to generate dendritic bursts, become place cells, and establish networks that store memories [28,71,72]. However, interneurons also target other interneurons, creating positive feedback loops that can support the

induction of long-term potentiation and associative learning and memory [73,74]. Interrupting these disinhibitory loops might then be the key. In this regard, the first class of interneurons that comes to mind are those that express vasoactive intestinal peptide (VIP+ INs), since they preferentially target other interneurons. However, VIP+ INs were reported to not express α5-$GABA_A$Rs in human or mouse prefrontal cortex [75], and an examination of the distribution of Gabra5 mRNA in hippocampal CA1 interneurons using a previously published database [76] confirms that this is the case in hippocampus as well, as Gabra5 levels are lowest in Vip+ of all interneuron classes (Fig. S8). On the other end of Gabra5 expression spectrum stands Cck+ basket cells – their Gabra5 expression levels are the highest of all (Fig. S8), they are densely expressed in dorsal CA1 [77], and their selective activation has been shown to enhance memory [78]. Therefore, depression of Cck+ basket cells via α5-$GABA_A$Rs is one possible mechanism. Neurogliaform and ivy cells also express Gabra5, at intermediate levels (Fig. S8), and they also receive $GABA_A$R-mediated slow IPSCs [79], which on pyramidal neurons are mediated by α5-$GABA_A$Rs [28,63,80]. In addition, they have high-density release sites, and they inhibit other interneurons as well as pyramidal cells via firing patterns that are time-locked to the theta oscillation [79,81]. Therefore, these cells may also be involved. Finally, Sst+ INs, which receive α5-$GABA_A$R,$_{slow}$ IPSCs [82] and play essential roles in the formation and control of contextual fear conditioning [83,84], are also good candidates for the control of learning and memory through interneuronal α5-$GABA_A$Rs.

A role for α5-$GABA_A$Rs located on interneurons in controlling hippocampus-dependent memory may have wide ramifications. Changes in α5-$GABA_A$R expression or activation have been proposed to contribute to memory deficits in Alzheimer's disease, schizophrenia, autism, aging, and in the early postoperative period [22,85-89]. Even if they are not the pathological basis *per se*, modulation of α5-$GABA_A$Rs has also been found effective in preclinical models of depression and Down syndrome [19-21]. It should be noted that our findings also support important roles for α5-$GABA_A$Rs on pyramidal neurons; indeed, there is evidence that pyramidal neuron α5-$GABA_A$Rs specifically regulate certain memory domains [44]. However, most studies focused on cognition have assumed that effects come from direct modulation of pyramidal neurons; the idea that they might derive instead (or in addition) from modulation of interneurons opens interesting possibilities. For example, modulation of α5-$GABA_A$Rs on different cell types might help explain why both α5-PAMs and α5-NAMs show efficacy in treatment of animal models of depression [18,19,21]. The recognition that α5-$GABA_A$Rs on interneurons are essential components of the hippocampal memory machinery, together with an emerging understanding of the functional diversity of interneurons, should present new opportunities for discovery and development of targeted therapeutics.

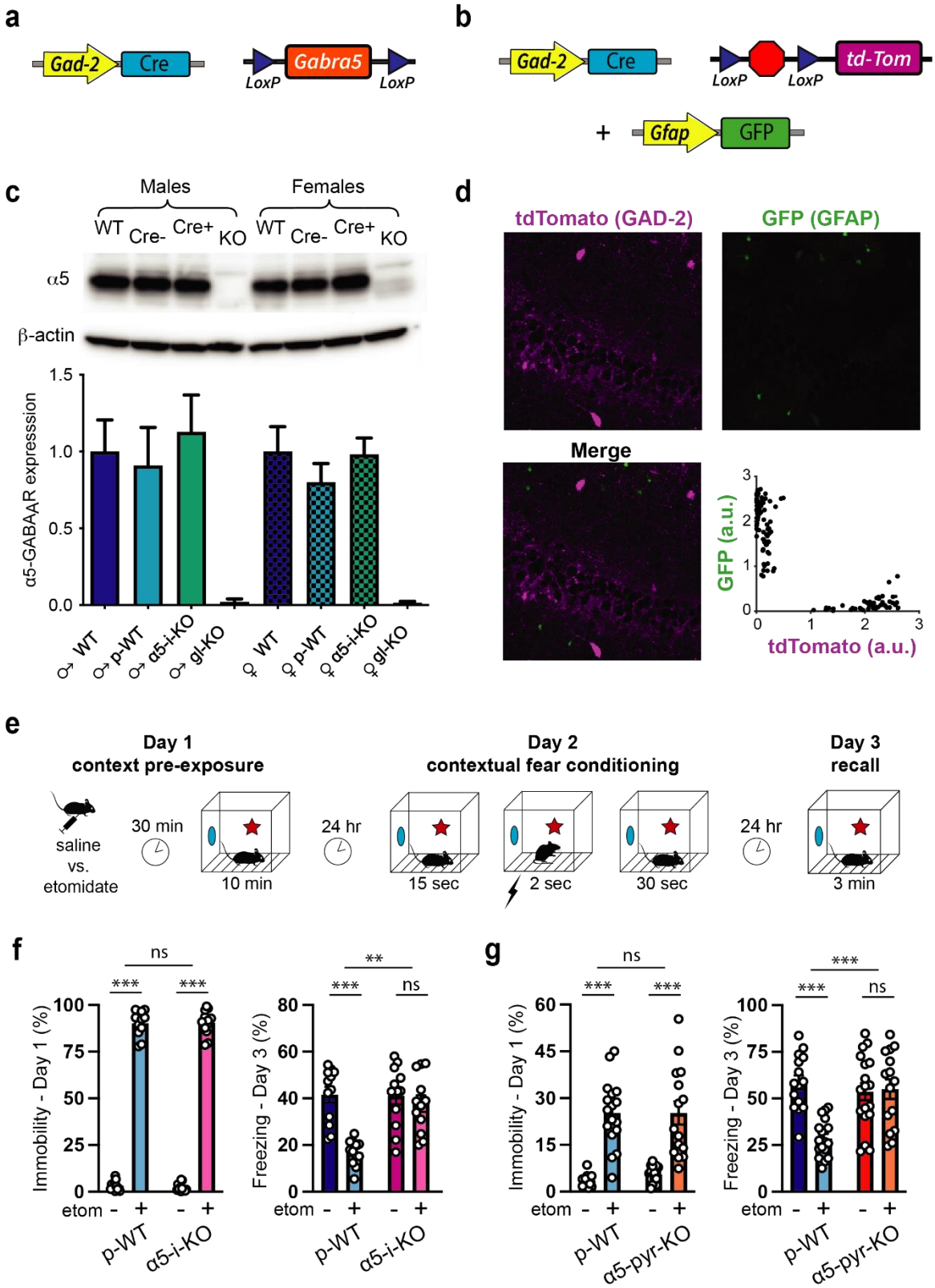
a
Gad-2
Cre
Gabra5
LoxP
LoxP
b
Gad-2
Cre
td-Tom
LoxP
LoxP
+
Gfap
GFP
c
Males
Females
WT
Cre-
Cre+
KO
WT
Cre-
Cre+
KO
α5
β-actin
α5-GABAAR expresssion
1.5
1.0
0.5
0.0
♂ WT
♂ p-WT
♂ α5-i-KO
♂ gl-KO
♀ WT
♀ p-WT
♀ α5-i-KO
♀ gl-KO
d
tdTomato (GAD-2)
GFP (GFAP)
Merge
GFP (a.u.)
tdTomato (a.u.)
e
Day 1
context pre-exposure
Day 2
contextual fear conditioning
Day 3
recall
saline
vs.
etomidate
30 min
10 min
24 hr
15 sec
2 sec
30 sec
24 hr
3 min
f
ns
***
***
**
***
ns
Immobility - Day 1 (%)
Freezing - Day 3 (%)
etom - + - +
p-WT
α5-i-KO
g
ns
***
***
***
***
ns
Immobility - Day 1 (%)
Freezing - Day 3 (%)
etom - + - +
p-WT
α5-pyr-KO

Fig. 1 | Mice lacking interneuronal α5-$GABA_A$Rs (α5-i-KO) resist memory suppression. a, Genetic strategy used to eliminate α5-$GABA_A$Rs from interneurons. Cre recombinase driven by the interneuron-specific Gad-2 promoter was used to target a floxed Gabra5 gene. **b,** Genetic strategy used to test overlap between Cre recombinase expression in interneurons (Cre-dependent td-Tomato expression) versus astrocytes (GFP driven by the astrocyte-specific Gfap promoter). **c,** Western blot analysis of α5-$GABA_A$R (55 kDa) expression in male and female C57BL6/J (WT), global knockout (gl-KO) mice, pseudo-WT (Cre-), and α5-i-KO (Cre+) mice. Expression levels were normalized to β-actin (42 kDa) and quantified by densitometry. Note that receptor levels were unchanged in Cre+ and Cre- mice versus WT mice, consistent with maintained expression in pyramidal neurons. **d,** Confocal imaging of transgene expression. Fluorescence levels (a.u.-arbitrary units) of Gad2-Cre driven td-Tom expression and Gfap-driven GFP expression were highly segregated, demonstrating a lack of Gad2-driven Cre recombinase in astrocytes. **e,** Context Pre-exposure Facilitation Effect (CPFE) behavioral paradigm used to assess etomidate suppression of contextual learning. **f,** *left,* Sedation levels (reduced mobility) during the 10-min pre-exposure session (day 1). Etomidate reduced mobility similarly in p-WT and α5-i-KO mice. *right,* Freezing scores during the recall session (day 3). Etomidate differentially suppressed freezing in p-WT *versus* α5-i-KO mice. **g,** *left*, Etomidate reduced mobility similarly in p-WT and α5-pyr-KO mice. *right*, Etomidate differentially suppressed freezing in p-WT versus α5-pyr-KO mice. $^{**}p<0.01$, $^{***}p<0.001$, n=12-18 mice/group.

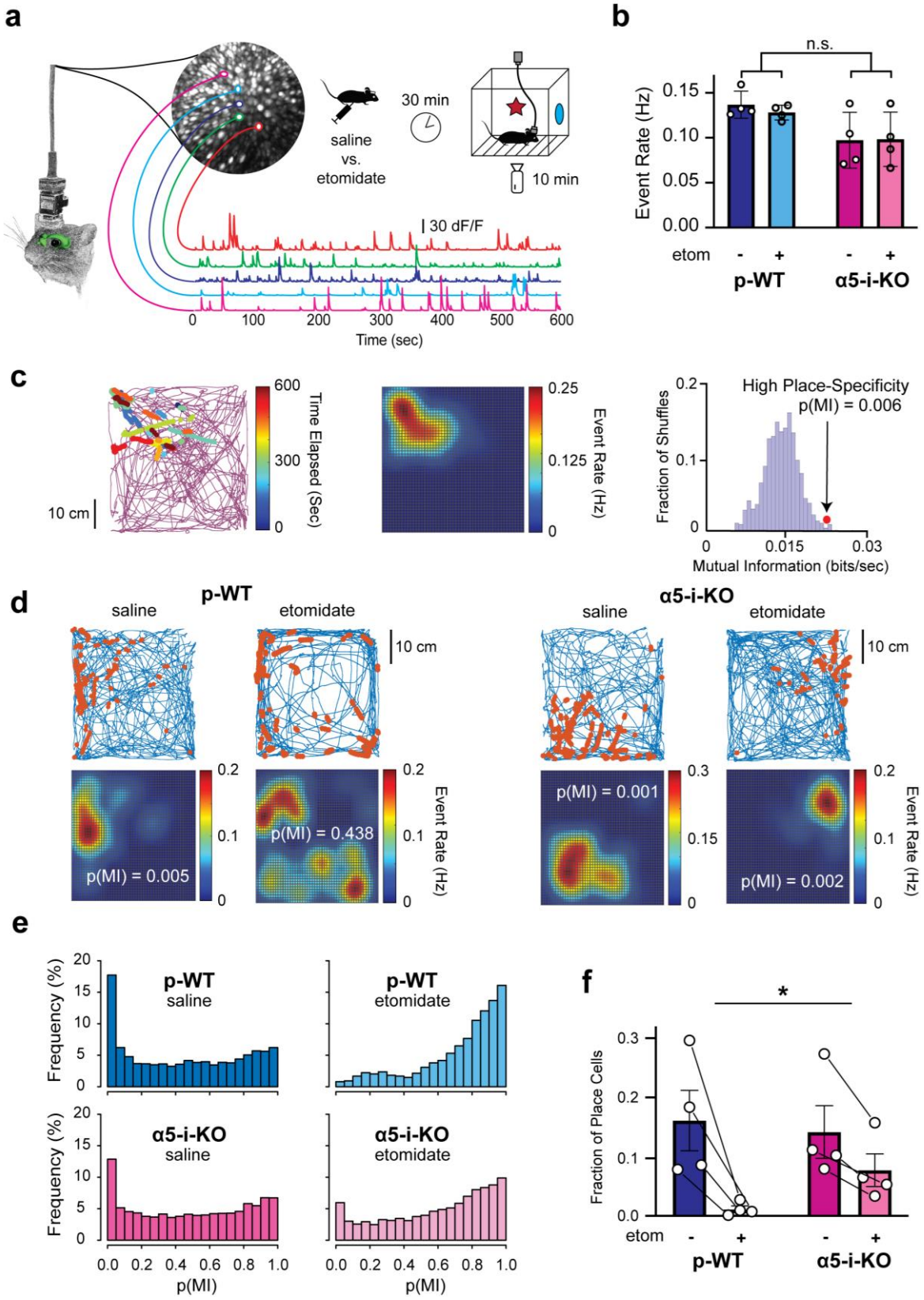
a
saline
vs.
etomidate
30 min
10 min
30 dF/F
0
100
200
300
400
500
600
Time (sec)
b
n.s.
Event Rate (Hz)
0.15
0.10
0.05
0.00
etom
-
+
-
+
p-WT
α5-i-KO
c
600
300
0
Time Elapsed (Sec)
10 cm
0.25
0.125
0
Event Rate (Hz)
High Place-Specificity
p(MI) = 0.006
Fraction of Shuffles
0.2
0.1
0
0.015
0.03
Mutual Information (bits/sec)
d
p-WT
saline
etomidate
α5-i-KO
saline
etomidate
10 cm
10 cm
0.2
0.1
0
p(MI) = 0.005
p(MI) = 0.438
0.3
0.15
p(MI) = 0.001
p(MI) = 0.002
Event Rate (Hz)
e
Frequency (%)
20
15
10
5
0
p-WT
saline
p-WT
etomidate
α5-i-KO
saline
α5-i-KO
etomidate
0.0
0.2
0.4
0.6
0.8
1.0
p(MI)
f
*
Fraction of Place Cells
0.3
0.2
0.1
0.0
etom
-
+
-
+
p-WT
α5-i-KO

Fig. 2 | Suppression of place cells by etomidate is attenuated in α5-i-KO mice. a, Hippocampal CA1 pyramidal neuron activity was measured using a head-mounted miniaturized endoscope to monitor AAV1-CaMKIIa-gCaMP6f fluorescence. Contours of five cells are overlayed on the maximum projected image from a 10-minute recording; their associated fluorescence traces are shown below. **(Inset)** Experimental paradigm used to evaluate place cell formation. Mice were administered saline or etomidate (2-8 mg/kg IP) 30 minutes before being placed in a square arena enriched with sensory cues. Ca^{2+} dynamics and arena location were captured simultaneously. **b**, Ca^{2+} event rates did not differ by genotype and were not altered by etomidate. **c**, Quantification of place-specific firing. **(Left panel)** Firing map of an individual cell with highly place-specific activity. The continuous purple line shows the path of the mouse in the experimental arena. Each string of dots represents a single Ca^{2+} event; the number of dots reflects the event amplitude distributed along the rising phase of the Ca^{2+} transient; string color designates the time at which the event occurred. **(Middle panel)** Gaussian-smoothed (filter radius = 8cm, sigma = 6cm) event rate map. **(Right panel)** Mutual information (MI) between mouse position and event rate, versus a time-shuffled null distribution, was used to quantify place-specificity. In this example, the probability of the observed MI (red dot) falling within the null distribution was p(MI)=0.006. **d**, Examples of firing maps and associated rate maps, showing low p(MI) (high place specificity) in both genotypes after saline, weak place specificity in p-WT mouse given etomidate 7 mg/kg, and maintained place specificity in α5-i-KO mouse given etomidate. **e**, Distributions of p(MI) values for all experiments under each condition. **f**, Fraction of cells with $p(MI)<0.05$ (i.e. place cells) in p-WT and α5-i-KO mice given saline or 7 mg/kg etomidate. Etomidate reduced the fraction of place cells in both genotypes, but the effect was attenuated in α5-i-KO mice (linear mixed effect model, genotype x drug interaction factor, $\chi^2(1) = 4.49$, $p=0.048$). *$p<0.05$, n=3-6 recordings from each of 4 mice/genotype for each drug condition (saline vs. etomidate 7mg/kg).

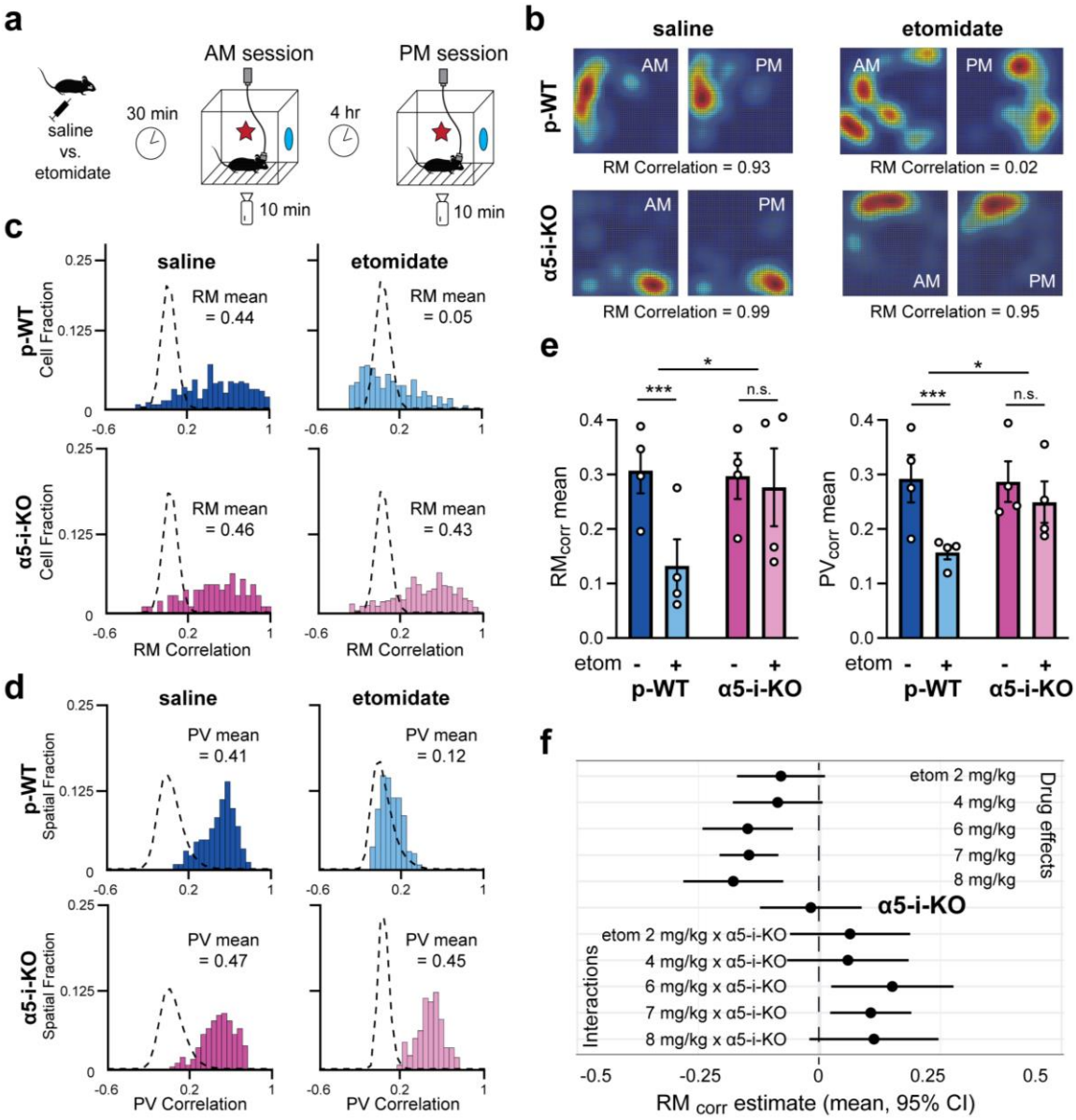

Fig. 3 | Suppression of spatial engram formation and/or stability by etomidate in WT but not α5-i-KO mice. a, Experimental paradigm used to assess engram formation. The same mice used to assess place cell formation (Fig. 2) were re-exposed to the same contexts for PM recording sessions. **b**, Examples of rate maps for individual neurons from p-WT (top) and α5-i-KO mice (bottom), administered saline (left) or 7mg/kg etomidate (right). Their associated rate map (RM) correlation coefficients between AM&PM sessions are shown below. **c**,**d**, Distributions of rate map (RM) and population vector (PV) correlation coefficients from single experiments (AM & PM sessions) in p-WT (top) and α5-i-KO mice (bottom), administered saline (left) or 7mg/kg etomidate (right). Note that distributions fell substantially to the right of the position-shuffled (RM) and vector-identity-shuffled (PV) null distributions (dashed lines) following saline administration, revealing the presence of a stable engram. Etomidate caused the distributions to be shifted toward the null distributions in p-WT mice but not α5-i-KO mice. **e**, Average RM_{corr} (left) and PV_{corr} (right) values from all mice. Each point represents the average of 3-6 AM&PM sessions under each condition. *p<0.05, ***p<0.001, n=4 mice/genotype. **f**, RM_{corr} estimates derived from linear mixed effects model for etomidate at doses ranging from 2-8 mg/kg vs saline.

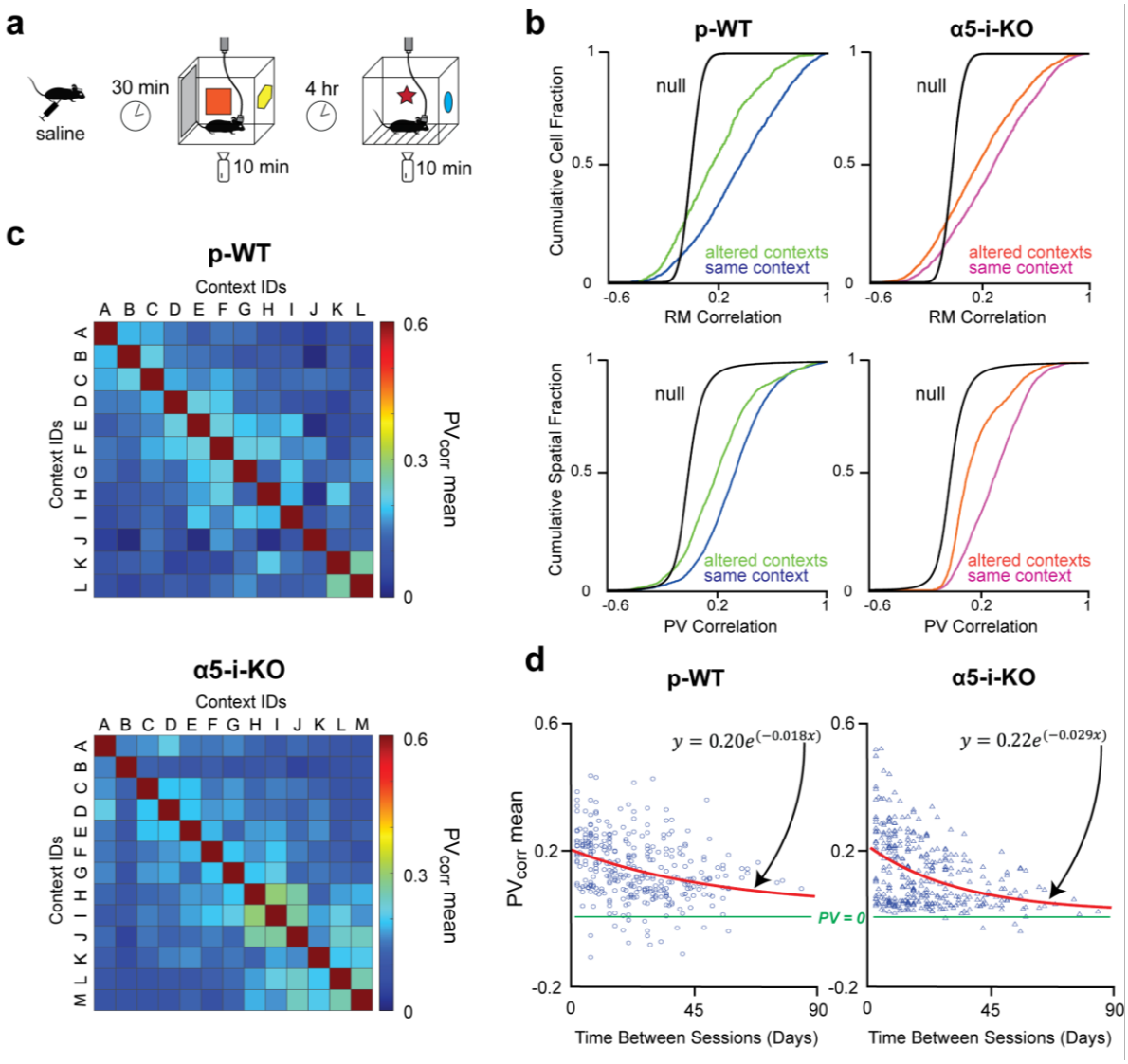

Fig. 4 | Context specificity of spatial engrams assessed by altered-context and cross-day correlation analysis. a, Experimental paradigm used to investigate context specificity of PV and RM correlations as memory correlates. **b**, Empirical cumulative distributions of RM (top) and PV (bottom) correlations for all cells in mice exposed to same or altered contexts. Correlation values were significantly lower for altered compared to same context experiments in p-WT mice for both RM and PV correlations, and a trend toward significance in α5-i-KO mice. **c**, Mean PV correlations across days for PM recording sessions, in mice administered either saline or etomidate in the AM. Mice were exposed to 12 distinct contexts across the span of ~90 days, and the mean PV was calculated between each pair of contexts (e.g. context A & B, or C & F). Mean PV correlations are summarized as a heatmap. The diagonal of identity has a value of '1', and upper right and lower left corners represent sessions furthest apart in time. Note that PV correlations are greater for pairs of session closer in time. **d**, Mean PV correlation between distinct spatial contexts as a function of time. Both genotypes show decreased correlations as a function of time interval between sessions.

Acknowledgments:

Funding:

National Institutes of Health grant R01 GM118801 (RAP)

National Institutes of Health grant 1R01GM128183 (UR and RAP)

National Institutes of Health grant U54HD090256 (UW-Madison, Waisman Center Core)

National Institutes of Health grant 1S10OD025040-01 (UW-Madison, Shared Instrumentation Facility)

National Institutes of Health grants MH061876 and NS097362 (ERC)

National Institutes of Health grant RO1-MH62122 (MSF)

E.R.C. is an Investigator of the Howard Hughes Medical Institute

Author contributions:

Conceptualization: RAP

Methodology: MZ, AA, MGP, BMK, RL, DR, HH, ERC, RN, UR, MSF, RAP

Investigation: MZ, AA, MGP, RL, DR, RN, RAP

Funding acquisition: ERC, UR, MSF, RAP

Supervision: ERC, UR, MSF, RAP

Writing – original draft: MZ, RAP

Writing – review & editing: MZ, AA, MGP, BMK, RL, DR, HH, ERC, RN, UR, MSF, RAP

Competing interests:

Authors declare that they have no competing interests.

Data and materials availability:

All data, code, and materials used in the analysis will be made available upon request.

Additional Information:

Supplementary Figures (Fig. S1-8).

References (Main text and supplementary text combined)

1. Olsen RW: GABA(A) receptor: Positive and negative allosteric modulators. Neuropharmacology 2018; 136: 10-22
2. Engin E, Benham RS, Rudolph U: An Emerging Circuit Pharmacology of GABAA Receptors. Trends Pharmacol Sci 2018; 39: 710-732
3. Ghoneim MM, Block RI: Learning and memory during general anesthesia: an update. [Review] [152 refs]. Anesthesiology 1997; 87: 387-410
4. Sandin RH, Enlund G, Samuelsson P, Lennmarken C: Awareness during anaesthesia: a prospective case study. The Lancet 2000; 355: 707-711
5. Mashour GA, Shanks A, Tremper KK, Kheterpal S, Turner CR, Ramachandran SK, Picton P, Schueller C, Morris M, Vandervest JC, Lin N, Avidan MS: Prevention of intraoperative awareness with explicit recall in an unselected surgical population: a randomized comparative effectiveness trial. Anesthesiology 2012; 117: 717-25
6. Osterman JE, Hopper J, Heran WJ, Keane TM, van der Kolk BA: Awareness under anesthesia and the development of posttraumatic stress disorder. Gen Hosp Psychiatry 2001; 23: 198-204
7. Benkwitz C, Liao M, Laster MJ, Sonner JM, Eger EI, 2nd, Pearce RA: Determination of the EC50 amnesic concentration of etomidate and its diffusion profile in brain tissue: implications for in vitro studies. Anesthesiology 2007; 106: 114-23
8. Forman SA: Clinical and molecular pharmacology of etomidate. Anesthesiology 2011; 114: 695-707
9. Cheng VY, Martin LJ, Elliott EM, Kim JH, Mount HT, Taverna FA, Roder JC, MacDonald JF, Bhambri A, Collinson N, Wafford KA, Orser BA: Alpha5GABAA receptors mediate the amnestic but not sedative-hypnotic effects of the general anesthetic etomidate. Journal of Neuroscience 2006; 26: 3713-3720
10. Martin LJ, Oh GH, Orser BA: Etomidate targets alpha5 gamma-aminobutyric acid subtype A receptors to regulate synaptic plasticity and memory blockade. Anesthesiology 2009; 111: 1025-1035
11. Sur C, Quirk K, Dewar D, Atack J, McKernan R: Rat and human hippocampal alpha5 subunit-containing gamma-aminobutyric AcidA receptors have alpha5 beta3 gamma2 pharmacological characteristics. Molecular Pharmacology 1998; 54: 928-933
12. Sur C, Fresu L, Howell O, McKernan RM, Atack JR: Autoradiographic localization of alpha5 subunit-containing GABAA receptors in rat brain. Brain Research 1999; 822: 265-270
13. Tulving E, Markowitsch HJ: Episodic and declarative memory: role of the hippocampus. Hippocampus 1998; 8: 198-204
14. Chambers MS, Atack JR, Broughton HB, Collinson N, Cook S, Dawson GR, Hobbs SC, Marshall G, Maubach KA, Pillai GV, Reeve AJ, MacLeod AM: Identification of a novel, selective GABA(A) alpha5 receptor inverse agonist which enhances cognition. J.Med.Chem. 2003; 46: 2227-2240
15. Chambers MS, Atack JR, Carling RW, Collinson N, Cook SM, Dawson GR, Ferris P, Hobbs SC, O'Connor D, Marshall G, Rycroft W, MacLeod AM: An orally bioavailable, functionally selective inverse agonist at the benzodiazepine site of GABAA alpha5 receptors with cognition enhancing properties. J.Med.Chem. 2004; 47: 5829-5832

16. Atack JR: Preclinical and clinical pharmacology of the GABAA receptor alpha5 subtype-selective inverse agonist alpha5IA. Pharmacol Ther 2010; 125: 11-26

17. Santrac A, Stamenic TT, Batinic B, Matovic BD, Stankovic T, Poe M, Cook J, Savic MM: Effect of MP-III-022, positive modulator of alpha 5 containing GABAA receptors, on learning and memory, European Neuropsychopharmacology, 2019, pp S173-S174

18. Prevot TD, Li G, Vidojevic A, Misquitta KA, Fee C, Santrac A, Knutson DE, Stephen MR, Kodali R, Zahn NM, Arnold LA, Scholze P, Fisher JL, Markovic BD, Banasr M, Cook JM, Savic M, Sibille E: Novel Benzodiazepine-Like Ligands with Various Anxiolytic, Antidepressant, or Pro-Cognitive Profiles. Mol Neuropsychiatry 2019; 5: 84-97

19. Fischell J, Van Dyke AM, Kvarta MD, LeGates TA, Thompson SM: Rapid Antidepressant Action and Restoration of Excitatory Synaptic Strength After Chronic Stress by Negative Modulators of Alpha5-Containing GABAA Receptors. Neuropsychopharmacology 2015; 40: 2499-509

20. Martinez-Cue C, Martinez P, Rueda N, Vidal R, Garcia S, Vidal V, Corrales A, Montero JA, Pazos A, Florez J, Gasser R, Thomas AW, Honer M, Knoflach F, Trejo JL, Wettstein JG, Hernandez MC: Reducing GABAA alpha5 Receptor-Mediated Inhibition Rescues Functional and Neuromorphological Deficits in a Mouse Model of Down Syndrome. Journal of Neuroscience 2013; 33: 3953-3966

21. Zanos P, Nelson ME, Highland JN, Krimmel SR, Georgiou P, Gould TD, Thompson SM: A Negative Allosteric Modulator for alpha5 Subunit-Containing GABA Receptors Exerts a Rapid and Persistent Antidepressant-Like Action without the Side Effects of the NMDA Receptor Antagonist Ketamine in Mice. eNeuro 2017; 4

22. Zurek AA, Kemp SW, Aga Z, Walker S, Milenkovic M, Ramsey AJ, Sibille E, Scherer SW, Orser BA: α5GABAA receptor deficiency causes autism-like behaviors. Ann Clin Transl Neurol 2016; 3: 392-8

23. Prevot T, Sibille E: Altered GABA-mediated information processing and cognitive dysfunctions in depression and other brain disorders. Mol Psychiatry 2020

24. Dawson GR, Maubach KA, Collinson N, Cobain M, Everitt BJ, MacLeod AM, Choudhury HI, McDonald LM, Pillai G, Rycroft W, Smith AJ, Sternfeld F, Tattersall FD, Wafford KA, Reynolds DS, Seabrook GR, Atack JR: An inverse agonist selective for alpha5 subunit-containing GABAA receptors enhances cognition. J Pharmacol Exp Ther 2006; 316: 1335-45

25. Gill KM, Grace AA: The role of alpha5 GABAA receptor agonists in the treatment of cognitive deficits in schizophrenia. Curr Pharm Des 2014; 20: 5069-76

26. Maramai S, Benchekroun M, Ward SE, Atack JR: Subtype Selective gamma-Aminobutyric Acid Type A Receptor (GABA(A)R) Modulators Acting at the Benzodiazepine Binding Site: An Update. Journal of Medicinal Chemistry 2020; 63: 3425-3446

27. Sperk G, Schwarzer C, Tsunashima K, Fuchs K, Sieghart W: GABA(A) receptor subunits in the rat hippocampus I: immunocytochemical distribution of 13 subunits. Neuroscience 1997; 80: 987-1000

28. Schulz JM, Knoflach F, Hernandez MC, Bischofberger J: Dendrite-targeting interneurons control synaptic NMDA-receptor activation via nonlinear alpha5-GABAA receptors. Nat Commun 2018; 9: 3576

29. Salesse C, Mueller CL, Chamberland S, Topolnik L: Age-dependent remodelling of inhibitory synapses onto hippocampal CA1 oriens-lacunosum moleculare interneurons. J Physiol 2011; 589: 4885-901

30. Petrache AL, Khan AA, Nicholson MW, Monaco A, Kuta-Siejkowska M, Haider S, Hilton S, Jovanovic JN, Ali AB: Selective Modulation of α5 GABA(A) Receptors Exacerbates Aberrant Inhibition at Key Hippocampal Neuronal Circuits in APP Mouse Model of Alzheimer's Disease. Front Cell Neurosci 2020; 14: 568194

31. Rodgers FC, Zarnowska ED, Laha KT, Engin E, Zeller A, Keist R, Rudolph U, Pearce RA: Etomidate Impairs Long-Term Potentiation In Vitro by Targeting alpha5-Subunit Containing GABAA Receptors on Nonpyramidal Cells. J Neurosci 2015; 35: 9707-16

32. Zarnowska ED, Rodgers FC, Oh I, Rau V, Lor C, Laha KT, Jurd R, Rudolph U, Eger EIN, Pearce RA: Etomidate blocks LTP and impairs learning but does not enhance tonic inhibition in mice carrying the N265M point mutation in the beta3 subunit of the GABA(A) receptor. Neuropharmacology 2015; 93: 171-178

33. Figueroa AG, Benkwitz C, Surges G, Kunz N, Homanics GE, Pearce RA: Hippocampal β2-GABA(A) receptors mediate LTP suppression by etomidate and contribute to long-lasting feedback but not feedforward inhibition of pyramidal neurons. J Neurophysiol 2021; 126: 1090-1100

34. Atack JR, Bayley PJ, Seabrook GR, Wafford KA, McKernan RM, Dawson GR: L-655,708 enhances cognition in rats but is not proconvulsant at a dose selective for alpha5-containing GABAA receptors. Neuropharmacology 2006; 51: 1023-9

35. Mederos S, Perea G: GABAergic-astrocyte signaling: A refinement of inhibitory brain networks. Glia 2019; 67: 1842-1851

36. Yavas E, Trott JM, Fanselow MS: Sexually dimorphic muscarinic acetylcholine receptor modulation of contextual fear learning in the dentate gyrus. Neurobiol Learn Mem 2021; 185: 107528

37. Rudy JW: Context representations, context functions, and the parahippocampal-hippocampal system. Learn Mem 2009; 16: 573-85

38. Miller LA, Heroux NA, Stanton ME: NMDA receptors and the ontogeny of post-shock and retention freezing during contextual fear conditioning. Dev Psychobiol 2020; 62: 380-385

39. Pinizzotto CC, Heroux NA, Horgan CJ, Stanton ME: Role of dorsal and ventral hippocampal muscarinic receptor activity in acquisition and retention of contextual fear conditioning. Behav Neurosci 2020; 134: 460-470

40. Fanselow MS: Factors governing one-trial contextual conditioning. Animal Learning & Behavior 1990; 18: 364-270

41. Fanselow MS: Contextual fear, gestalt memories, and the hippocampus. Behav Brain Res 2000; 110: 73-81

42. Krasne FB, Cushman JD, Fanselow MS: A Bayesian context fear learning algorithm/automaton. Front Behav Neurosci 2015; 9: 112

43. Tsien JZ, Huerta PT, Tonegawa S: The essential role of hippocampal CA1 NMDA receptor-dependent synaptic plasticity in spatial memory. Cell 1996; 87: 1327-1338

44. Engin E, Sigal M, Benke D, Zeller A, Rudolph U: Bidirectional regulation of distinct memory domains by alpha 5-subunit-containing GABA(A) receptors in CA1 pyramidal neurons. Learning & Memory 2020; 27: 423-428

45. O'Keefe J, Nadel L: The hippocampus as a cognitive map. Oxford, Clarendon Press, 1978

46. Grieves RM, Jeffery KJ: The representation of space in the brain. Behav Processes 2017; 135: 113-131

47. O'Keefe J, Dostrovsky J: The hippocampus as a spatial map. Preliminary evidence from unit activity in the freely-moving rat. Brain Research 1971; 34: 171-175

48. Wilson MA, McNaughton BL: Dynamics of the hippocampal ensemble code for space. Science 1993; 261: 1055-1058

49. Kentros C, Hargreaves E, Hawkins RD, Kandel ER, Shapiro M, Muller RV: Abolition of long-term stability of new hippocampal place cell maps by NMDA receptor blockade. Science. 1998; 280: 2121-2126

50. Thompson LT, Best PJ: Long-term stability of the place-field activity of single units recorded from the dorsal hippocampuus of freely behaving rats. Brain Research 1990; 509: 299-308

51. Muller RU, Kubie JL: The effects of changes in the environment on the spatial firing of hippocampal complex-spike cells. J Neurosci 1987; 7: 1951-68

52. Anderson MI, Jeffery KJ: Heterogeneous modulation of place cell firing by changes in context. J Neurosci 2003; 23: 8827-35

53. Ziv Y, Burns LD, Cocker ED, Hamel EO, Ghosh KK, Kitch LJ, El Gamal A, Schnitzer MJ: Long-term dynamics of CA1 hippocampal place codes. Nat Neurosci 2013; 16: 264-6

54. Sheintuch L, Geva N, Baumer H, Rechavi Y, Rubin A, Ziv Y: Multiple Maps of the Same Spatial Context Can Stably Coexist in the Mouse Hippocampus. Curr Biol 2020; 30: 1467-1476 e6

55. Sheintuch L, Rubin A, Brande-Eilat N, Geva N, Sadeh N, Pinchasof O, Ziv Y: Tracking the Same Neurons across Multiple Days in Ca(2+) Imaging Data. Cell Rep 2017; 21: 1102-1115

56. Rubin A, Sheintuch L, Brande-Eilat N, Pinchasof O, Rechavi Y, Geva N, Ziv Y: Revealing neural correlates of behavior without behavioral measurements. Nat Commun 2019; 10: 4745

57. Tanaka KZ, He H, Tomar A, Niisato K, Huang AJY, McHugh TJ: The hippocampal engram maps experience but not place. Science 2018; 361: 392-397

58. Stefanini F, Kushnir L, Jimenez JC, Jennings JH, Woods NI, Stuber GD, Kheirbek MA, Hen R, Fusi S: A Distributed Neural Code in the Dentate Gyrus and in CA1. Neuron 2020; 107: 703-716 e4

59. Kinsky NR, Sullivan DW, Mau W, Hasselmo ME, Eichenbaum HB: Hippocampal Place Fields Maintain a Coherent and Flexible Map across Long Timescales. Curr Biol 2018; 28: 3578-3588 e6

60. Bullmore E, Sporns O: Complex brain networks: graph theoretical analysis of structural and functional systems. Nat Rev Neurosci 2009; 10: 186-98

61. Kim JJ, Fanselow MS: Modality-specific retrograde amnesia of fear. Science 1992; 256: 675-677

62. Orser BA: Lifting the fog around anesthesia. Sci Am 2007; 296: 54-61

63. Zarnowska ED, Keist R, Rudolph U, Pearce RA: GABAA receptor alpha5 subunits contribute to GABAA,slow synaptic inhibition in mouse hippocampus. J Neurophysiol 2009; 101: 1179-91

64. Ali AB, Thomson AM: Synaptic alpha 5 subunit-containing GABAA receptors mediate IPSPs elicited by dendrite-preferring cells in rat neocortex. Cereb.Cortex 2008; 18: 1260-1271

65. Robinson NTM, Descamps LAL, Russell LE, Buchholz MO, Bicknell BA, Antonov GK, Lau JYN, Nutbrown R, Schmidt-Hieber C, Hausser M: Targeted Activation of Hippocampal Place Cells Drives Memory-Guided Spatial Behavior. Cell 2020; 183: 1586-1599 e10

66. Josselyn SA, Tonegawa S: Memory engrams: Recalling the past and imagining the future. Science 2020; 367

67. Ghandour K, Ohkawa N, Fung CCA, Asai H, Saitoh Y, Takekawa T, Okubo-Suzuki R, Soya S, Nishizono H, Matsuo M, Osanai M, Sato M, Ohkura M, Nakai J, Hayashi Y, Sakurai T, Kitamura T, Fukai T, Inokuchi K: Orchestrated ensemble activities constitute a hippocampal memory engram. Nat Commun 2019; 10: 2637

68. Rubin A, Geva N, Sheintuch L, Ziv Y: Hippocampal ensemble dynamics timestamp events in long-term memory. Elife 2015; 4

69. Tonegawa S, Liu X, Ramirez S, Redondo R: Memory Engram Cells Have Come of Age. Neuron 2015; 87: 918-31

70. Hunsaker MR, Kesner RP: Unfolding the cognitive map: The role of hippocampal and extra-hippocampal substrates based on a systems analysis of spatial processing. Neurobiol Learn Mem 2018; 147: 90-119

71. Bittner KC, Milstein AD, Grienberger C, Romani S, Magee JC: Behavioral time scale synaptic plasticity underlies CA1 place fields. Science 2017; 357: 1033-1036

72. Geiller T, Sadeh S, Rolotti SV, Blockus H, Vancura B, Negrean A, Murray AJ, Rozsa B, Polleux F, Clopath C, Losonczy A: Local circuit amplification of spatial selectivity in the hippocampus. Nature 2021

73. Letzkus JJ, Wolff SB, Luthi A: Disinhibition, a Circuit Mechanism for Associative Learning and Memory. Neuron 2015; 88: 264-76

74. Leao RN, Mikulovic S, Leao KE, Munguba H, Gezelius H, Enjin A, Patra K, Eriksson A, Loew LM, Tort AB, Kullander K: OLM interneurons differentially modulate CA3 and entorhinal inputs to hippocampal CA1 neurons. Nat Neurosci 2012; 15: 1524-30

75. Hu X, Rocco BR, Fee C, Sibille E: Cell Type-Specific Gene Expression of Alpha 5 Subunit-Containing Gamma-Aminobutyric Acid Subtype A Receptors in Human and Mouse Frontal Cortex. Mol Neuropsychiatry 2019; 4: 204-215

76. Harris KD, Hochgerner H, Skene NG, Magno L, Katona L, Bengtsson Gonzales C, Somogyi P, Kessaris N, Linnarsson S, Hjerling-Leffler J: Classes and continua of hippocampal CA1 inhibitory neurons revealed by single-cell transcriptomics. PLoS Biol 2018; 16: e2006387

77. Whissell PD, Cajanding JD, Fogel N, Kim JC: Comparative density of CCK- and PV-GABA cells within the cortex and hippocampus. Front Neuroanat 2015; 9: 124

78. Whissell PD, Bang JY, Khan I, Xie YF, Parfitt GM, Grenon M, Plummer NW, Jensen P, Bonin RP, Kim JC: Selective Activation of Cholecystokinin-Expressing GABA (CCK-GABA) Neurons Enhances Memory and Cognition. eNeuro 2019; 6

79. Capogna M, Pearce RA: GABAA, slow: causes and consequences. Trends in Neurosciences 2011; 34: 101-112

80. Prenosil GA, Schneider Gasser EM, Rudolph U, Keist R, Fritschy JM, Vogt KE: Specific subtypes of GABAA receptors mediate phasic and tonic forms of inhibition in hippocampal pyramidal neurons. J Neurophysiol. 2006; 96: 846-857

81. Olah S, Komlosi G, Szabadics J, Varga C, Toth E, Barzo P, Tamas G: Output of neurogliaform cells to various neuron types in the human and rat cerebral cortex. Front Neural Circuits 2007; 1: 4

82. Magnin E, Francavilla R, Amalyan S, Gervais E, David LS, Luo X, Topolnik L: Input-Specific Synaptic Location and Function of the alpha5 GABAA Receptor Subunit in the Mouse CA1 Hippocampal Neurons. J Neurosci 2019; 39: 788-801

83. Lovett-Barron M, Kaifosh P, Kheirbek MA, Danielson N, Zaremba JD, Reardon TR, Turi GF, Hen R, Zemelman BV, Losonczy A: Dendritic inhibition in the hippocampus supports fear learning. Science 2014; 343: 857-63

84. Szonyi A, Sos KE, Nyilas R, Schlingloff D, Domonkos A, Takacs VT, Posfai B, Hegedus P, Priestley JB, Gundlach AL, Gulyas AI, Varga V, Losonczy A, Freund TF, Nyiri G: Brainstem nucleus incertus controls contextual memory formation. Science 2019; 364

85. Hauser J, Rudolph U, Keist R, Mohler H, Feldon J, Yee BK: Hippocampal alpha5 subunit-containing GABAA receptors modulate the expression of prepulse inhibition. Mol.Psychiatry 2005; 10: 201-207

86. Gill KM, Lodge DJ, Cook JM, Aras S, Grace AA: A novel alpha5GABA(A)R-positive allosteric modulator reverses hyperactivation of the dopamine system in the MAM model of schizophrenia. Neuropsychopharmacology 2011; 36: 1903-11

87. Schmid LC, Mittag M, Poll S, Steffen J, Wagner J, Geis HR, Schwarz I, Schmidt B, Schwarz MK, Remy S, Fuhrmann M: Dysfunction of Somatostatin-Positive Interneurons Associated with Memory Deficits in an Alzheimer's Disease Model. Neuron 2016; 92: 114-125

88. Zurek AA, Yu J, Wang DS, Haffey SC, Bridgwater EM, Penna A, Lecker I, Lei G, Chang T, Salter EW, Orser BA: Sustained increase in α5GABAA receptor function impairs memory after anesthesia. J Clin Invest 2014; 124: 5437-41

89. Koh MT, Rosenzweig-Lipson S, Gallagher M: Selective GABA(A) alpha5 positive allosteric modulators improve cognitive function in aged rats with memory impairment. Neuropharmacology 2013; 64: 145-52

90. Cushman JD, Maldonado J, Kwon EE, Garcia AD, Fan G, Imura T, Sofroniew MV, Fanselow MS: Juvenile neurogenesis makes essential contributions to adult brain structure and plays a sex-dependent role in fear memories. Front Behav Neurosci 2012; 6: 3

91. Zhou P, Resendez SL, Rodriguez-Romaguera J, Jimenez JC, Neufeld SQ, Giovannucci A, Friedrich J, Pnevmatikakis EA, Stuber GD, Hen R, Kheirbek MA, Sabatini BL, Kass RE, Paninski L: Efficient and accurate extraction of in vivo calcium signals from microendoscopic video data. Elife 2018; 7

92. Friedrich J, Zhou P, Paninski L: Fast online deconvolution of calcium imaging data. PLoS Comput Biol 2017; 13: e1005423

93. Chen TW, Wardill TJ, Sun Y, Pulver SR, Renninger SL, Baohan A, Schreiter ER, Kerr RA, Orger MB, Jayaraman V, Looger LL, Svoboda K, Kim DS: Ultrasensitive fluorescent proteins for imaging neuronal activity. Nature 2013; 499: 295-300

94. Olypher AV, Lánský P, Muller RU, Fenton AA: Quantifying location-specific information in the discharge of rat hippocampal place cells. Journal of Neuroscience Methods 2003; 127: 123-135

95. Bates D, Maechler M, Bolker B, Walker S: Fitting Linear Mixed-Effects Models Using lme4. Journal of Statistical Software 2015; 67: 1-48

Methods

Animals. All experiments were conducted under the oversight and with the approval of the Institutional Animal Care and Use Committee (IACUC) of the University of Wisconsin-Madison. Experiments were conducted on a total of 95 mice from the Gad2-cre ($Gad2^{tm2(cre)Zjh}$) x α5-floxed ($Gabra5^{tm2.1Uru}$) line, and 3 wild type C57BL6/J mice. Mice of both sexes were used for behavioral experiments (45 males, 42 females). Only male mice were used for the GCaMP6f imaging because their larger size facilitated lens and baseplate implantation.

All mice were generated and maintained on the C57BL/6J background. Pseudo-WT (p-WT) and their interneuron-specific Gabra5 knockout littermates (α5-i-KO) were created in a three-step process. F0 mice were homozygous α5-floxed (α5:fl/fl) and hemizygous Gad2-cre (JAX strain # 010802) or VIAAT-cre (JAX strain # 017535) mice obtained from the Jackson Laboratory (Bar Harbor, Maine, USA). As expected, F1 offspring were all heterozygous for the α5-floxed gene (α5:fl/-) and approximately one-half were also hemizygous for the Gad2-cre or VIAAT-cre gene. F2 mice were created by crossing a F1 α5:fl/-;cre+ mouse and a F1 α5:fl/-;cre- mouse. F3 mice were created by crossing F2 mice that were homozygous for α5-floxed gene (α5:fl/fl;cre-) with F2 mice also homozygous for α5-floxed gene plus hemizygous for Gad2-cre or VIAAT-cre (α5:fl/fl;cre+). F3 mice consisting of (α5:fl/fl;cre+) and (α5:fl/fl;cre-) were used as breeding pairs. Experimental mice came from F3 breeding pairs and subsequent generations produced by the same strategy (α5:fl/fl;cre+) x (α5:fl/fl;cre-).

We monitored for germ-line recombination by testing for the presence of Cre recombinase plus the α5-floxed allele, the α5-KO allele, and the α5-WT allele. Any mice that were negative for Cre recombinase but positive for the α5-KO allele were considered to have undergone germ-line recombination. We observed a high rate of germ-line recombination in the VIAAT-cre x α5-floxed line, whether Cre was carried by the male or female (~25% of offspring), but never any germ-line recombination in the Ga2-cre x α5-floxed line, whether Cre was carried by the male or female. Therefore, all experiments were conducted using only mice from the Gad2 line.

Genotyping. Mice were genotyped from tail samples either in-house using traditional, gel based PCR methods, or sent to Transnetyx (Cordova, TN), which uses a TaqMan-based assay for real-time PCR data. For in-house PCR, primers purchased from IDT (Integrated DNA Technologies, Coralville, IA) were as follows (forward, reverse):
Gabra5: TGATGGCACACTTCTCTACACC, CTTTGAAAGCATTTCCCGAAGC;
Gad2-cre: CTAGGCCACAGAATTGAAAGATCT,GTAGGTGGAAATTCTAGCATCATCC;
Viaat-cre: GCGGTCTGGCAGTAAAAACTATC, GTGAAACAGCATTGCTGTCACTT.

Ex-vivo microscopy. To image fluorescent markers td-Tomato and GFP, coronal slices (100-400 um thickness) were cut from three mice and imaged live in cold, oxygenated ACSF. Hippocampal subfields were imaged on an Olympus FluoView FV1000 upright confocal microscope with a water immersion objective (either a LUMPlanFl/IR 40X N.A.=0.8, or a XLUMPLFL 20X N.A.=1.00). Z-series images (at least 40-50μm in Z) were acquired with 488nm and 561nm laser lines (sequential excitation). Several dozen fluorophore-expressing cells were observed in each volume of interest. From these z-series, the cell bodies of fluorophore-

expressing cells (either td-Tomato or GFP) were segmented, and average fluorescence (a.u.) in each color was quantified.

Western blot analysis. A 1:2 dilution of supernatant of the anti-α5-$GABA_A$R NeuroMab clone N415/24 was used. There were three animals per genotype and gender. Single animals from each group were run per gel (3 gels total). Expression levels were quantified by densitometry and normalized to β-actin (42 kDa). The means from the three WT males or three WT females, corrected for β-actin levels, were set to 1.0.

Behavioral experiments. Behavioral studies were carried out at the Waisman Center Rodent Models Core facility at the University of Wisconsin-Madison. Mice were transferred from the primary animal care unit in which they were bred and raised to the Waisman Center animal care unit at least one week prior to initiating behavioral experiments. Studies of contextual fear conditioning were carried out first, followed by elevated plus maze, and then thermal sensitivity, with 3-4 days between experiments.

Context Preexposure Facilitation Effect (CPFE). We used a preexposure-dependent contextual fear conditioning paradigm adapted from Cushman et al., 2012 [90]. This paradigm, which is often referred to in the literature as the Context Preexposure Facilitation Effect (CPFE) paradigm [37-39] takes advantage of the so-called "immediate shock deficit" [36,40], wherein animals that are shocked immediately (within several seconds) upon entry into a novel environment do not freeze on subsequent re-exposure, whereas mice that had been exposed on a prior day do exhibit a freezing response. The proposed explanation is that preexposed mice establish a hippocampus-dependent representation of the environment (i.e. contextual memory), which takes several minutes, and this pre-formed memory can be recalled rapidly on reexposure for subsequent association with the aversive stimulus [41,42]. This paradigm was chosen because etomidate, as an anesthetic, might suppress freezing to context during a standard contextual conditioning paradigm, not by preventing the formation of a contextual memory (a hippocampus-dependent process), but rather by reducing the aversive nature of the shock, or some other aspect of its ability to support aversive conditioning. By administering etomidate during the context exposure phase, separated by one day from the shock exposure phase, that interpretive ambiguity is removed.

The CPFE experiments took place over two weeks. During the first week, the mice were habituated and handled in the behavioral testing room for 10 min a day. During the second week, the mice underwent three experimental phases – context preexposure, conditioning, and recall – on three consecutive days. Mice were brought into the behavioral testing room 30 minutes prior to the testing procedure. On day 1 (*context preexposure*), mice were injected with either saline or etomidate (7 mg/kg *i.p.*), placed back in their home cage for 30 minutes, and then placed into the test chamber for 10 minutes. The test chamber was 20 cm x 20 cm x 30 cm high, constructed of clear acrylic with checkered patterned paper covering three of the four walls and a shock grid floor consisting of stainless-steel bars 2 cm apart, diameter 2 mm. On day 2 (*conditioning*), mice were placed into the same test chamber, and after 15 s they were administered a single foot-shock (2 s, 1 mA). The mice remained in the test chamber for an additional 30 s (47 s total time) and they were then returned to their home cage. On day 3 (*recall*), mice were placed in the test chamber for 8 min. The amount of time they spent moving was recorded using FreezeFrame™ software. The percentage of time they were 'immobile' (movement below a pre-defined

threshold level) on day 1 served as a measure of drug-induced sedation; the percentage of time that they were immobile during the first three minutes of the drug-free test on experimental day 3 ('freezing behavior') served as a quantitative measure of fear memory.

Elevated Plus Maze (EPM) Test. Mice were placed individually in a plus-shaped maze composed of two "open" arms without walls (30 cm L X 5 cm W) and two closed arms (30 cm L X 5 cm W) enclosed by walls (10 cm H) arranged around a center zone (5 cm L X 5 cm W). Over the course of five minutes, the amount of time they spent on the arms and the number of entries to each arm were manually recorded by an experimenter blind to the genotype of the mice. The percent time the animal spent on the open arms and the number of entries to each arm served as a measure of anxiety-like behavior, with more entries and more time spent on the open arms indicating less anxiety.

Hotplate Test. An electronically controlled hotplate (30 cm L X 30 cm W) heated to 55 °C was used to measure sensitivity to a noxious thermal stimulus. The hot plate was turned on 30 minutes prior to testing to ensure that the desired temperature was reached. Mice were then placed individually on the hot-plate and the latency to elicit a nocifensive behavior (e.g., hind paw withdrawal or licking) was manually recorded by the experimenter blinded to the genotype of the mice.

Open Field Test (OFT). Mice were placed individually in a square chamber (40 cm X 40 cm X 30 cm) and allowed to move freely for 10 minutes. The total distance that each mouse traveled was measured using *Fusion*™ software (Omnitech Electronics Inc.).

Ca^{2+} Imaging Experiments. Eight male mice (4 p-WT, 4 α5-i-KO) each underwent two stereotaxic surgeries separated by 2-3 weeks. For both procedures, mice were anesthetized with isoflurane ~2% adjusted to maintain immobility and spontaneous ventilation and warmed by block heater to maintain normothermia. Postoperatively mice received a subcutaneous injection of carprofen 5mg/kg. For the first surgery, a small craniotomy window was made over the right dorsal hippocampus (from bregma: AP =-2.0, ML =-1.6) and 500 nL of virus carrying the genetically encoded calcium indicator GCaMP6f driven by the CaMKIIa promoter (Inscopix Ready-to-Image AAV1-CaMKIIa-GCaMP6f) was injected at DV =-1.6 at a rate of 80 nL/min using a NanoFil syringe with a 35g needle driven by a UMP3 microsyringe pump and SMARTouch controller (WPI). The needle was kept in place for 2 min, then retracted 200um, where it remained for an additional 8 min before removing slowly. The skin was sutured closed, and the mouse was observed during recovery from surgery and anesthesia then returned to its home cage. For the second surgery, which took place 2-3 weeks later, a larger craniotomy was made at AP=-2.2, ML=-2.1, and the cortex corpus callosum overlaying the hippocampus was aspirated using a 30g blunt needle and cold saline irrigation, taking care not to aspirate the alveus. Once bleeding was controlled with Gelfoam and cold saline irrigation, an integrated GRIN lens (1 mm diameter x 4 mm length) and baseplate were inserted slowly at a 9 deg angle to the midline, until the center of the surface of the lens rested DV=-1.2. The baseplate was cemented in place using Metabond, the surrounding skin was sutured closed, and the mouse was allowed to recover from surgery and anesthesia, then returned to its home cage.

Two to three weeks later, a miniature epifluorescence microscope (Inscopix nVoke) was affixed to the baseplate, and the mouse was placed in the behavioral arena (a 40 cm x 40 cm x 30

cm tall acrylic enclosure) surrounded by blackout curtain, with exam table paper placed on the floor of the arena, and allowed to explore freely for 10 minutes. A commutator (Inscopix) was used to prevent tangling of the wire attached to the microscope. During this initial 'screening session', the focal plane, illumination, and gain were adjusted to identify the optimal settings to observe cellular activity. If the number of cells with sufficient activity levels was too low (fewer than 60 cells with >5 Ca^{2+} events) the mouse was returned to its home cage and tested one week later. Once sufficient activity was observed, which typically occurred 5-6 weeks following the initial surgery with virus injection, the same settings were used for all subsequent recording sessions, except that the illumination was occasionally adjusted down or up to maintain appropriate fluorescent signal levels.

On each experimental day, two recording sessions separated by 4 hrs (AM and PM sessions, 10 min each) took place in the same behavioral arena used for the initial screening sessions. For the AM session, the arena contained a unique set of visual, olfactory, and tactile cues forming a 'novel context'. Visual cues consisted of 8"x11" sheets of paper mounted onto the outsides of all four walls, with different solid colors, shapes (stars, circles, squares, triangles) and patterns (stripes, swirls, lines) on the four sheets. Olfactory cues consisted of 1 μL of odorant (benzaldehyde, hexanal, alpha-pinene, heptaldehyde, eugenol, or eucalyptol) on filter paper placed within a 35mm covered culture dish and set in one corner of the arena. Tactile cues consisted of ¼" thick acrylic squares covering one quarter of the arena floor, or various sizes of shallow glass petri dish lids placed either open side up or down, in addition to a sheet of exam table paper covering the floor of the entire arena. Prior to the AM session, a mouse received either saline (control) or etomidate (2-8 mg/kg) by intraperitoneal injection, carried out in a separate room. Thirty minutes after the injection the mouse was brought into the recording room, the miniature microscope was attached to the baseplate, the mouse was placed in the arena, and the light in the arena was turned down to ~2 lux to encourage exploration. A bank of infrared lights above the mouse (12 lux) was used to illuminate the arena so that the mouse could be tracked using an IR-sensitive camera (Basler aca1300-60gm) mounted below the arena (Fig. 2A). The video camera and epifluorescent microscopy acquisition were synchronized using a hardware trigger controlled by Ethovision software (Noldus Information Technology). At the end of the 10-min recording session, the miniature microscope was detached, and the mouse was returned to its home cage in a separate room. For the PM session, the mouse was brought back into the recording room, the miniature microscope was mounted to the baseplate, and the mouse was placed back into the arena containing the same set of sensory cues used for the AM session.

Experiments using a novel set of cues for the AM session and unchanged cues for the PM session took place 2-3 times per week, with at least on day between experiments. In separate sets of control experiments, different sets of sensory cues were used for the AM and PM sessions ("alternate context" experiments), or PM sessions were omitted, and mice were re-exposed to the same set of sensory cues the following day ("24-hour memory" experiments). For each mouse, experiments continued for up to 8 weeks (14 weeks post-virus injection), at which time the number of cells with sufficient activity was typically declining.

Behavioral tracking recordings were analyzed using Noldus EthoVision XT15 and exported as csv files. These csv files summarized the mice's XY-location (body center) as a function of time. All behavioral tracking csv files were organized into a specific data structure with experimental time, animal ID, genotype, and related experimental conditions. The in-vivo calcium imaging recordings were also organized into a matching data structure. An excel

metadata sheet for all animals and all experiments allows for programmatic reference (MATLAB 2021a).

Place Cell and Spatial Engram Analysis. Calcium imaging recordings were analyzed in two stages. The first stage utilized the MATLAB API package embedded within Inscopix Data Processing Software v1.6.0 (IDPS v1.6.0). Each recording was 'preprocessed' to remove artifacts, then downsampled both spatially and temporally by a factor of two. Preprocessed recordings were spatially filtered (low cutoff = 0.005 $pixel^{-1}$; high cutoff = 0.5 $pixel^{-1}$) to remove low and high spatial frequency content for better contrast and smoother frames, and frames were motion-corrected based on a region of interest (ROI) that contained blood vessels as background references. To improve visualization of calcium events and to generate a maximum projected image for estimation of average cell diameter (needed for subsequent analysis using the CNMF-E algorithm), a ΔF/F transformation was applied. Fluorescent signals were then quantified by deviations from background noise. The constrained nonnegative matrix factorization for microendoscopic data (CNMF-E) image analysis method was applied to the processed recording, with analysis parameters optimized according to Zhou et al., 2018 [91]. The noisy calcium traces of detected cells were deconvolved using the 'online active set method to infer spikes' (OASIS) method [92]. Once deconvolved, calcium traces were event-detected based on biokinetics of GCaMP6f, using a threshold of 3 median absolute deviations (MAD) [93] to establish 'cellsets' of calcium events. Several analyzed cellsets were randomly chosen to verify that inferred spikes accurately reflected calcium signals from detected cells, based on visual inspection. To be included in further analysis, only those cells with exactly one spatial component, appropriate size, and more than 5 detected calcium events were accepted. Finally, cellsets of all recordings obtained from an individual mouse were longitudinally registered, so that the activity of each unique cell could be traced between and across recording sessions [55]. These data were exported as csv files that included cell global ID, the timestamps (beginning of rising phase) of inferred calcium spikes, and the fluorescence amplitude of calcium spikes in MAD.

For the second stage of analysis, we used custom-written MATLAB functions to merge behavioral tracking and calcium event data to characterize place cells and spatial engrams (Fig. S3). ***Behavioral tracking analysis***: (1) speed was calculated based on XY-location and smoothed with a triangular window (size=0.5 sec); (2) the fraction of time that the mouse spent actively exploring (speed > 2 cm/sec) was calculated; (3) an occupancy-time map (sec) was created by dividing the arena into a 10-by-10 matrix (i.e. 100 pixels), and computing the duration that a mouse spent within each pixel. ***Place cell analysis*** (Fig. S3A): (1) calcium event timestamps were matched with behavioral tracking timestamps in order to find the spatial location of the mouse at the onset of each calcium event; (2) calcium events that occurred during periods of inactivity (speed < 2cm/sec) were excluded from analysis; (3) for each cell, an amplitude-weighted *calcium event map* was created by duplicating calcium events according to their amplitudes (~1-8 MAD) and distributing them along the track of the mouse, at intervals of 40 ms, for the duration of the rising phase of the GCaMP6f fluorescence signal. (4) for each cell, a *calcium event rate map* (events/sec; 10-by-10 matrix) was created by dividing the calcium event map by the occupancy-time map, pixel-by-pixel; (5) for each cell, the mutual information (MI) between the calcium event rate map and occupancy-time map for each cell was calculated according to the formulae:

$$I_{pos}(x_i) = \sum_{K \geq 0} P_{k|x_i} \, log_2(\frac{P_{k|x_i}}{P_k})$$

$$MI = \sum_{i=1} P_{x_i} I_{pos}(x_i)$$

Where:

- x_i refers to one pixel in the binned arena (in our analysis, the arena is depicted by a 10-by-10 matrix).
- $I_{pos}(x_i)$ is the positional information (in bits) of pixel x_i.
- P_{x_i} is the probability that the mouse occupies pixel x_i, calculated as ($\frac{time\ spent\ in\ x_i}{total\ time\ of\ recording}$).
- P_k is the probability of observing k calcium events
- $P_{k|x_i}$ is the conditional probability of observing k calcium events in pixel x_i, which is equivalent to calcium event rate in pixel x_i.
- MI is the mutual information (in bits per second) between calcium event rate and mouse's spatial location.

(adapted from: [59,94]; (6) for each cell, a null distribution of time-shuffled MI values was created by 1000 random circular permutations of calcium event timestamps; this null distribution was used to calculate p(MI). ***Rate Map (RM) Correlation*** (Fig. S3B): (1) for each cell, calcium event rate maps were smoothed by a Gaussian filter (radius = 10 cm, sigma = 6 cm) to generate smoothed calcium event rate maps; (2) for each cell, Pearson's correlation coefficient (PCC) was calculated between the vectorized smoothed calcium event rate maps from AM and PM sessions (or more broadly, between any two arbitrarily chosen sessions); (3) to detect and account for possible coherent rotation of cells' event rate maps [59], we calculated RM correlation by rotating maps from one session only (either AM or PM) by 0°, 90°, 180°, and 270°, and the rotation that resulted in maximum mean(RM) was designated as angle of coherent rotation—which usually was 0° (Fig. S4); (4) for each pair of sessions, the distribution of PCCs from all coactive cells (i.e. those with >5 calcium events during both sessions) was referred to as RM correlation distribution; (5) for each pair of sessions, a null distribution of RM correlation values was created by 100 random spatial permutations of smoothed calcium rate maps. ***Population Vector (PV) Correlation*** (Fig. S3C): (1) for each pair of sessions, smoothed calcium event rate maps of all coactive cells were organized into two 3-dimensional matrices, thus forming for each pixel a pair of population vectors (PVs); (2) for each pixel, the PCC between the two PVs was calculated, resulting in a PV correlation distribution; (3) to detect and account for coherent rotation, we calculated PV correlation by using the same rotation procedure as in RM correlation computation, and again an angle of coherent rotation based on PV is determined—which again usually was 0° (though RM and PV did not always agree) (Fig. S4); (4) for each pair of sessions, a null distribution of PV correlation values was created by 100 random permutations of PVs for all pixels.

Data Presentation and Statistical Analysis. Statistical comparisons for contextual learning studies were made using 2-way ANOVA followed by Šídák's multiple comparisons test (CPFE sedation and freezing, saline vs. etomidate in p-WT vs. α5-i-KO), or Welch's t test (pre-exposure vs. no-pre-exposure, elevated plus maze, hot plate tests)(Graphpad Prism v. 9.2.0). Comparisons for Ca^{2+} imaging data were made by fitting linear mixed effects models [95] using RStudio, 2021.09.0 Build 351 (R Core Team (2021). R: A language and environment for statistical computing. R Foundation for Statistical Computing, Vienna, Austria. URL https://www.R-project.org/.) and applying t-tests or maximum likelihood tests, as indicated.